Euro. Jnl of Applied Mathematics (1997), *vol.* 8, *pp.* 311–329. Printed in the United Kingdom

© 1997 Cambridge University Press

Two-dimensional Stokes flows with time-dependent free boundaries driven by surface tension

S. RICHARDSON

Department of Mathematics and Statistics, University of Edinburgh, Scotland

(*Received 15 May 1996; revised 28 November 1996*)

We consider the two-dimensional quasi-steady Stokes flow of an incompressible Newtonian fluid occupying a time-dependent simply-connected region bounded by a free surface, the motion being driven solely by a constant surface tension acting at the free boundary. Of particular concern here are such flows that start from an initial configuration with the fluid occupying an array of touching circular disks. We show that, when there are N such disks in a general position, the evolution of the fluid region is described by a conformal map involving $2N-1$ time-dependent parameters whose variation is governed by N invariants and $N-1$ first order differential equations. When $N = 2$, or when the problem enjoys some special features of symmetry, the moving boundary of the fluid domain during the motion can be determined by solving purely algebraic equations, the solution of a single differential equation being needed only to link a particular boundary shape to a particular time. The analysis is aided by exploiting a connection with Hele-Shaw free boundary flows when the zero-surface-tension model is employed. If the initial configuration for the Stokes flow problem can be produced by injection (or suction) at N points into an initially empty Hele-Shaw cell, as can the N-disk configuration referred to above, then so can all later configurations; the points where the fluid must be injected move, but the amount to be injected at each of the N points remains invariant. The efficacy of our solution procedure is illustrated by a number of examples, and we exploit the method to show that the free boundary in such a Stokes flow driven by surface tension alone may pass through a cusped state.

1 Introduction

The process known as *viscous sintering* is employed in several industrial contexts and has recently been the subject of much theoretical and numerical work. In its most basic form, a mass of Newtonian fluid surrounded entirely by a free surface is involved, and the motion is driven solely by the action of a constant surface tension acting at that free surface; gravitational and compressibility effects are negligible, and the relevant Reynolds numbers are extremely small. A useful survey of the ideas and associated techniques has been given by van de Vorst (1994).

A number of the problems of practical importance in the field are two-dimensional; one may envisage taking a bundle of solid fibres or cables, heating the assemblage until it becomes fluid, and then allowing surface tension to drive a flow that converts it into a single cylinder with a circular cross-section. That there exist explicit analytic solutions to a whole

https://doi.org/10.1017/S0956792597003057 Published online by Cambridge University Press

class of free boundary problems of this kind was first discovered by Hopper (1990), and subsequent publications by the same author (Hopper, 1991, 1992, 1993) confirm the utility of his methods. Independently, a similar approach to the analysis of such problems was developed by Richardson (1992) as an extension of his earlier work (Richardson, 1968, 1973) on time-independent flows to time-dependent situations.

A case of particular interest in the above context arises when the motion begins with a bundle of circular cylinders, so the two-dimensional problem concerns a fluid that is initially confined to an array of touching circular disks. In general, the cross-section to be dealt with may become multiply-connected, but we here confine attention to the motion when it is simply-connected. The fundamental problem involving the coalescence of two circular cylinders of the *same* radius was first solved by Hopper (1984), but presented in a simpler form by Hopper (1990). A solution for the coalescence of two circular cylinders of *different* radii was given by Richardson (1992) – but note that one of the conclusions of the present work is that the solution there is needlessly complicated. In this paper, we show that the evolution of any cross-section that begins as an array of touching circular disks and remains simply-connected can be described analytically in simple terms. With N initial disks, the fluid always occupies a region that is the image of a circular disk by a conformal map given by a rational function with just N simple poles; any arrangement of N touching circular disks can be produced as the limit of the image domains of a circular disk by an appropriate sequence of such rational maps. That this should be so follows from the results in Richardson (1997a) which considered Hele-Shaw free boundary flows driven by injection or suction, with a zero-surface-tension condition applied at the boundary. It was there shown how one could construct such flows with expanding blobs of fluid absorbing other isolated blobs or, reversing time, with shrinking blobs of fluid leaving isolated blobs behind; the behaviour of the conformal maps there is precisely what we need here, and they are given by rational functions with only simple poles. In fact, some of the examples of Hele-Shaw flows in Richardson (1996a, b, 1997b) also involve the same mathematical feature; the maps there are no longer given by rational functions because the global conditions are somewhat different, but the local behaviour of the map that produces the absorbing and disgorging phenomena is identical.

There are a number of connections between the viscous sintering and Hele-Shaw problems we have been discussing. If the initial state of either can be produced by injection (or suction) at N points into an initially empty Hele-Shaw cell, as is the case for the N-disk configuration of particular interest in the sintering context, then both situations involve conformal maps from the unit disk given by rational functions with just N simple poles. Thus every configuration through which the sintering problem passes can be produced by injecting *some* amount of fluid at *some* arrangement of N points in the Hele-Shaw analogue. In fact, we show that the amount of fluid to be injected remains invariant and only the positions of the points change. It is expedient to employ a convenient phraseology: when we speak of an injection point in the Hele-Shaw analogue moving to a neighbouring point, we envisage injection taking place at the latter simultaneously with suction at the former so that the net amount injected remains the same, until the contribution from the original point has been reduced to zero. Then the configurations through which the sintering evolves are given by moving the injection points in the Hele-Shaw analogue, while keeping the amounts injected fixed. For example, we obtain two touching circular disks of radii r_1

https://doi.org/10.1017/S0956792597003057 Published online by Cambridge University Press

and r_2 if we inject areas πr_1^2 and πr_2^2 into a Hele-Shaw cell at two points whose distance apart is r_1+r_2. The evolution of the region occupied by fluid in the corresponding sintering problem of the coalescence of two circular cylinders of radii r_1 and r_2 is given by simply moving these injection points closer together, while maintaining the areas injected as πr_1^2 and πr_2^2.

In §2, we examine the limiting forms of the image domains that result when we consider particular sequences of conformal maps, and investigate some mathematical aspects of this process that we need to exploit. §3 begins by recalling formulae that arise in an analysis of some Hele-Shaw free boundary flows when the zero-surface-tension model is employed, and shows how this setting adds some physical insight to help in understanding the mathematical phenomena discussed in §2. The corresponding formulae in the sintering context are summarized in §4, and the relationship between the sintering and Hele-Shaw scenarios is also established in this section. The viability of the resultant solution scheme for the Stokes flow problems is demonstrated in §5 by means of a number of examples; these are presented with a minimum of computational detail, but some comments on the numerical aspects appear in §6. One of the examples in §5 shows that the popular belief that the inclusion of surface tension at a free boundary will ensure that it remains smooth is not correct; even when surface tension is the sole agent driving the flow, a cusp may develop in the free boundary.

2 Limiting forms of conformal maps

Suppose $z = g(\zeta)$ yields a conformal map of the unit disk $|\zeta| < 1$ in the ζ-plane onto some domain D in the z-plane; we wish to examine the effect on this map of adding to $g(\zeta)$ a simple pole in $|\zeta| > 1$ that is allowed to approach some point $\zeta_0 = \mathrm{e}^{i\phi_0}$ on the unit circle $|\zeta| = 1$. It will be evident as we proceed that $g(\zeta)$ must be subject to some restrictions; to begin with, it might be simplest to think of $g(\zeta)$ as convex, but it should soon become clear that much weaker geometric conditions will suffice. We also suppose $g(\zeta)$ to be analytic at $\zeta = \zeta_0$ and require ∂D to have a well-defined tangent at $z_0 = g(\zeta_0)$; in particular, $g'(\zeta_0) \neq 0$. Choosing the notation with future applications in mind, consider the map given by a function $w(\zeta)$ of the form

$$z = w(\zeta) = g(\zeta) + \frac{\bar{\beta}\zeta}{1-\bar{\gamma}\zeta} \tag{2.1}$$

with β and γ two complex parameters such that $|\gamma| < 1$; an overbar denotes a complex conjugate. With no essential loss of generality, we may suppose the pole at $\zeta = 1/\bar{\gamma}$ in (2.1) to approach $\zeta_0 = \mathrm{e}^{i\phi_0}$ along a radius, and so write

$$\gamma = (1-\epsilon)\,\mathrm{e}^{i\phi_0}, \tag{2.2}$$

where $0 < \epsilon < 1$ and we are concerned with the limit $\epsilon \to 0+$. To ensure that the map given by $w(\zeta)$ in (2.1) does not blow up near $\zeta = \zeta_0$, we must have $\beta \to 0$ as $\epsilon \to 0+$; suppose that

$$\beta \sim b\epsilon\,\mathrm{e}^{i\psi_0} \quad \text{as} \quad \epsilon \to 0+ \tag{2.3}$$

for some real constant $b > 0$ and real argument ψ_0.

https://doi.org/10.1017/S0956792597003057 Published online by Cambridge University Press

If ζ lies outside some neighbourhood of ζ_0, then $w(\zeta)\to g(\zeta)$ as $\epsilon\to 0+$. To focus attention on the fate of the image of the portion of $|\zeta|=1$ near $\zeta=\zeta_0$ in this limit, set

$$\zeta = \mathrm{e}^{i(\phi_0+s\epsilon)} = \zeta_0\,\mathrm{e}^{is\epsilon}, \tag{2.4}$$

with s a real parameter. When we insert this into (2.1) and exploit (2.2) and (2.3), we find that letting $\epsilon\to 0+$ with $s=O(1)$ yields

$$z = g(\zeta_0) + b\,\mathrm{e}^{i(\phi_0-\psi_0)}\frac{1+is}{1+s^2}, \tag{2.5}$$

which is the parametric equation for a circle of radius $\frac{1}{2}b$ and centre at $z=g(\zeta_0)+\frac{1}{2}b\,\mathrm{e}^{i(\phi_0-\psi_0)}$; the point $z_0=g(\zeta_0)$ on this circle corresponds to $s\to\pm\infty$. To ensure that this circle does not encroach on the original domain D, the centre must lie on the outward normal to ∂D at $z_0=g(\zeta_0)$, so that we need

$$\psi_0 = -\arg\{g'(\zeta_0)\}. \tag{2.6}$$

With this condition in force, the limit of the domain onto which $w(\zeta)$ defined in (2.1) maps the unit disk $|\zeta|<1$ as $\epsilon\to 0+$ is composed of the original domain D furnished by $g(\zeta)$, together with a circular disk of radius $\frac{1}{2}b$ touching ∂D at $z_0=g(\zeta_0)$.

The relation (2.6) is a necessary condition for the univalence of the family of maps we are considering, a fact that can be seen in a different way. Not only does the pole of $w(\zeta)$ at $\zeta=1/\bar{\gamma}$ in (2.1) move to the point $\zeta=\zeta_0$ as $\epsilon\to 0+$, but so do two zeros of the derivative $w'(\zeta)$. These zeros are at ζ where

$$\zeta \sim \zeta_0 \pm i\epsilon^{1/2}\left\{\frac{b\,\mathrm{e}^{-i\psi_0}}{g'(\zeta_0)}\right\}^{1/2}\zeta_0 \quad \text{as} \quad \epsilon\to 0+, \tag{2.7}$$

and we see that (2.6) is a necessary condition for these zeros to remain in $|\zeta|>1$. The zeros move to $\zeta=\zeta_0$ somewhat more slowly than does the pole but, while we have supposed the pole to move along a radial path, the zeros approach tangentially. It is, of course, these zeros of $w'(\zeta)$ that produce the two cusps whose simultaneous formation and coalescence causes the circular disk to be cut off from D in the limit.

Two further features of the limiting process are important and will appear in a different guise later. If the circular disk that has been grafted on to the original domain D has its centre at $z=a$ and is of radius r, we find that

$$w(\gamma)\to a \quad \text{and} \quad \beta w'(\gamma)\to r^2; \tag{2.8}$$

as the pole of $w(\zeta)$ at $\zeta=1/\bar{\gamma}$ moves to the unit circle, the image of its inverse in the unit circle moves to the centre of the attached disk, while the dilatation at this inverse point tends to infinity.

It should now be evident that we can produce any array of touching circular disks as the limit of the domains produced by a sequence of rational maps with only simple poles by iterating the procedure embodied in (2.1); we begin with $g(\zeta)$ as a multiple of ζ or, more generally, as a bilinear function with its pole in $|\zeta|>1$, and continually update the meaning to be attributed to $g(\zeta)$ as we add further disks. We will see that the procedure requires a certain amount of care (besides the obvious constraints that must be imposed on the geometry to maintain univalence), but we first note that the idea is capable of considerable generalization.

https://doi.org/10.1017/S0956792597003057 Published online by Cambridge University Press

Suppose $z = g(\zeta)$ yields a conformal map of the unit disk $|\zeta| < 1$ onto a domain D, while $z = h(\zeta)$ yields a conformal map of this same disk onto a domain D'. Let $\zeta_0 = \mathrm{e}^{i\phi_0}$ and $\zeta_1 = \mathrm{e}^{i\phi_1}$ be points on $|\zeta| = 1$ and suppose $g(\zeta)$ to be analytic at $\zeta = \zeta_0$ with $g'(\zeta_0) \neq 0$, while $h(\zeta)$ is analytic at $\zeta = \zeta_1$ with $h'(\zeta_1) \neq 0$. Now consider D' to be translated so that the point $z_1 = h(\zeta_1)$ on $\partial D'$ is moved to coincidence with the point $z_0 = g(\zeta_0)$ on ∂D, and then rotated about this point so that the repositioned D' is disjoint from D; some evident geometric constraints on D and D' are necessary for this to be possible and for the machinery we are introducing to work as claimed, but we will not elaborate on these. The region given by taking the union of D and the relocated D' is then the limit of the image domains as $\epsilon \to 0+$ of the family of maps given by $z = w(\zeta; \epsilon)$ where

$$w(\zeta; \epsilon) = g(\zeta) - U\left\{h\left(\frac{\zeta_0 - (1+\epsilon)\,\zeta}{\zeta_0 - (1-\epsilon)\,\zeta}\zeta_1\right) - h(\zeta_1)\right\} \tag{2.9}$$

for $0 < \epsilon < 1$; here U is a factor of unit modulus whose sole purpose is to furnish the correct rotation, and so must be given by

$$U = \exp\{i[\phi_0 - \phi_1 + \arg g'(\zeta_0) - \arg h'(\zeta_1)]\}. \tag{2.10}$$

If D' is a circular disk of radius r that we wish to graft on to D, we can choose $h(\zeta) = r\zeta$, when equations (2.9) and (2.10) reduce to the original proposal embodied in (2.1), (2.2) and (2.3).

We present some pertinent examples, all intended to produce the same array of four circular disks, with a central one of radius 1.2 and three touching neighbours of radii 1.4, 1 and 0.8, these being such that the lines between the centre of the central disk and their own centres are at angles of 60°, 180° and 270°, respectively, in the anticlockwise sense from the positive x-direction, where $z = x + iy$.

With $g(\zeta)$ in (2.1) as 1.2ζ giving the central disk, the proposal gives us the family of maps

$$w(\zeta; \epsilon) = 1.2\zeta + \frac{2.8\,\epsilon\zeta}{1-(1-\epsilon)\,\mathrm{e}^{-i\pi/3}\zeta} + \frac{2\,\epsilon\zeta}{1+(1-\epsilon)\,\zeta} + \frac{1.6\,\epsilon\zeta}{1-(1-\epsilon)\,i\zeta}. \tag{2.11}$$

The image domains produced by this family as ϵ decreases from 0.4 in steps of 0.05 are shown at top-left in Figure 1; they behave as expected.

To illustrate the use of (2.9) and (2.10), together with some of the pitfalls of this idea, we consider a different way of generating this same array; think of it as the disk of radius 1 on the left, with the array of three disks on the right grafted on to it. The 3-disk array can be produced by the family of maps

$$h(\zeta; \epsilon) = 1.2\zeta + \frac{2.8\,\epsilon\zeta}{1-(1-\epsilon)\,\mathrm{e}^{-i\pi/3}\zeta} + \frac{1.6\,\epsilon\zeta}{1-(1-\epsilon)\,i\zeta}, \tag{2.12}$$

and we ought to be able to use the rationale behind (2.9) with $g(\zeta) = \zeta$ to produce the desired result. We can, but must note that the argument leading to (2.9) assumes that the map $h(\zeta)$ does not itself depend on ϵ, while the proposed formula in (2.12) demonstrably does. To obtain what we seek, we can use the family of maps

$$w(\zeta; \epsilon) = \zeta + h\left(-\frac{1-(1+\epsilon^2)\,\zeta}{1-(1-\epsilon^2)\,\zeta}; \epsilon\right) - h(-1; \epsilon), \tag{2.13}$$

https://doi.org/10.1017/S0956792597003057 Published online by Cambridge University Press

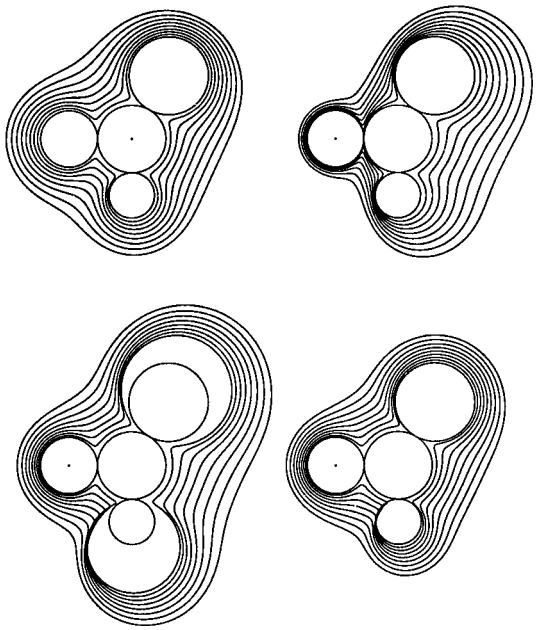


FIGURE 1. Four attempts to produce a sequence of maps whose image domains converge to a particular array of four touching circular disks, with a central disk of radius 1.2 and three neighbours of radii 1.4, 1 and 0.8. In each sketch, the point to which the origin of the ζ-plane is mapped is marked by a dot. See text for further details and the formulae used. All the boundaries are drawn for ϵ decreasing from 0.4 in steps of 0.05.

with $h(\zeta;\epsilon)$ given by (2.12); note the appearance of both ϵ^2 and ϵ here. Using (2.12) and (2.13), we obtain the result at top-right in Figure 1, which is as desired. If, however, we replace ϵ^2 by ϵ in the two places where it appears in (2.13), the effect is as shown in the sketch at bottom-left in Figure 1; the lower lobe shrinks down to a circle that is twice as large as expected, while the limit for the upper one is too large by a factor of 4/3. (If this procedure is used for a disk attached to that of radius 1.2 at an angle ϕ_0 to the positive x-direction, the limit is a factor $\sec^2(\phi_0/2)$ too large.) If we make allowances for this magnification by changing the numbers 2.8 and 1.6 in (2.12) to 2.1 and 0.8 respectively, then (2.13) with ϵ^2 replaced by ϵ performs as required, giving the result at bottom-right in Figure 1.

If we *interchange* the roles of ϵ^2 and ϵ in (2.13), the consequences are disastrous, as might be anticipated from the above observations; the family of maps is no longer univalent.

These examples show that the local behaviour of the maps we must use is quite complicated. Fortunately, the Hele-Shaw analogue to be considered in the next section will make a detailed examination of the singularities invoked unnecessary. Nevertheless, it is important to understand the basic features in order to appreciate the numerical difficulties involved, and to see how they may be alleviated. For example, the first scheme in Figure 1 maps the origin in the ζ-plane to the centre of the central disk, and the three outer disks are formed by three simple poles approaching three *different* points on the unit circle $|\zeta| = 1$. The other schemes in Figure 1 map the origin to the centre of the left-hand disk, and the

https://doi.org/10.1017/S0956792597003057 Published online by Cambridge University Press

3-disk array grafted onto it is formed by three simple poles (each with two attendant zeros of the derivative of the mapping function) all approaching the *same* point on $|\zeta| = 1$; the milder singularities produced by the first scheme are to be preferred. In general, one should endeavour to map the origin to a point near some notional centre of the array.

In all the examples illustrated in Figure 1, we have mapped the origin in the ζ-plane to the centre of one of the disks; equivalently, we have always taken $g(\zeta)$ in (2.1) or (2.9) as a simple multiple of ζ. Taking $g(\zeta)$ to be a more general bilinear function, we can arrange for the origin to map to some point within a disk other than its centre, but we will have no cause to take advantage of this freedom. However, there are instances when a different approach *is* helpful. If the array of disks is symmetric about a point where two disks touch, it is sensible to exploit this symmetry, which means that the origin of the ζ-plane must be chosen to map to this special point. This situation arises when we consider sintering with two equal circular cylinders, and the map used by Hopper (1990) to solve this problem enjoys this property. An analysis similar to that already described can be given for circumstances where this different choice is appropriate; it is similar to that used by Richardson (1992) when discussing the sintering of two unequal cylinders. We merely note here that, with an appropriate interpretation, both relations in (2.8) continue to hold, a fact that will become apparent from a different point of view in the next section.

3 Hele-Shaw flows

We describe the motion in a Hele-Shaw cell in terms of a projection on to a Cartesian (x, y)-plane that is parallel to the solid planes forming the cell, and have $z = x + iy$ as the usual complex variable. We suppose a constant pressure condition to be applicable at the free boundary (often thought of as a zero-surface-tension model), and consider an area πr_j^2 of fluid to have been injected into an initially empty cell at the point $z = a_j$ for $j = 1, 2, \ldots, N$; if suction has actually been applied at $z = a_j$ we simply take $r_j^2 < 0$. If the planform of the region occupied by fluid is simply-connected, then it is shown by Richardson (1997a) that it is the image of the unit disk $|\zeta| < 1$ by a conformal map $z = w(\zeta)$ given by a function of the form

$$w(\zeta) = \sum_{j=1}^{N} \frac{\bar{\beta}_j \zeta}{1 - \bar{\gamma}_j \zeta}, \tag{3.1}$$

where the $2N$ parameters β_j and γ_j for $j = 1, 2, \ldots, N$, with $|\gamma_j| < 1$, are subject to the $2N$ conditions

$$w(\gamma_j) = a_j \quad \text{and} \quad \beta_j w'(\gamma_j) = r_j^2 \quad \text{for} \quad j = 1, 2, \ldots, N. \tag{3.2}$$

In particular, the injection points are the images of the points in the ζ-plane that are the inverses in the unit circle $|\zeta| = 1$ of the poles in (3.1). Physical intuition now suggests a number of ways to produce a sequence of simply-connected domains as images of a sequence of maps of the form (3.1) whose limit gives us an array of N touching circular disks. If the disks have centres $z = a_j$ and radii r_j for $j = 1, 2, \ldots, N$, we can first inject areas πR_j^2 at $z = a_j$ where $R_j \geqslant r_j$ for $j = 1, 2, \ldots, N$, with $R_j > r_j$ for at least one j, and then apply suction to reduce the net amount injected at each $z = a_j$ to πr_j^2. The corresponding sequence of maps we obtain from (3.1) and (3.2) will then behave as required, provided some evident geometric constraints are satisfied to ensure univalence. An example successfully producing

https://doi.org/10.1017/S0956792597003057 Published online by Cambridge University Press

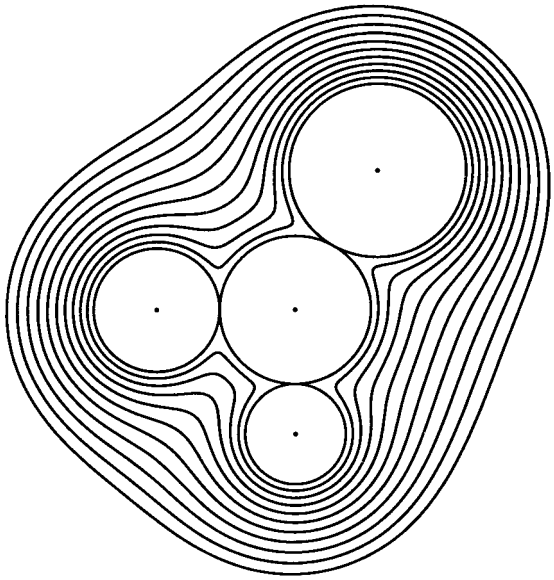


FIGURE 2. A sequence of maps converging to the same array of circular disks as in Figure 1, but produced by exploiting injection in a Hele-Shaw cell. The injection points marked by dots are at $z = 0, 2.6\,e^{i\pi/3}, -2.2$ and $-2i$ with amounts injected of $\pi(1.2+\epsilon)^2$, $\pi(1.4+\epsilon)^2$, $\pi(1+\epsilon)^2$ and $\pi(0.8+\epsilon)^2$, respectively. The boundaries are drawn for ϵ decreasing from 1 in steps of 0.1.

the same array of circular disks as was the objective in Figure 1 is shown in Figure 2. Here, the initial state contemplated above has $R_j > r_j$ for all relevant $j = 1, 2, 3$ and 4, and the subsequent suction occurs simultaneously at four points.

A different scheme to produce the array of N disks of radii r_j and centres at $z = a_j$ is closer to that we will need when discussing sintering; begin by injecting amounts πr_j^2 at N injection points that are close together, and then push these points apart to the locations $z = a_j$ while keeping invariant the amount injected at each. This involves solving the system (3.2) with the r_j fixed but the a_j varying, while the earlier scheme kept the a_j fixed and varied r_j. We are now moving the injection points in the Hele-Shaw problem in the sense defined in §1. It is, of course, possible to attain the desired aim of a given array of disks by varying both the position of the injection points and the amounts injected simultaneously.

In fact, the presentation of the above ideas has been a little too simplistic in an attempt to achieve clarity. A conformal map is not specified uniquely merely by giving the domain onto which the unit disk is to be mapped, so the $2N$ equations in (3.2) cannot be sufficient to determine the $2N$ parameters β_j and γ_j given the a_j and r_j. In a general situation, it is natural to take an injection point at the origin of the z-plane, say $a_1 = 0$. We can then choose to map the origin of the ζ-plane to this point, so that $\gamma_1 = 0$; the simple pole at $\zeta = 1/\bar{\gamma}_1$ in (3.1) has been taken to lie at infinity, there remain only $2N-1$ parameters in (3.1), and the first equation $w(0) = 0$ in (3.2) is now redundant. We can also impose the condition that $w'(0)$ be real and positive which, from the equation with $j = 1$ in the second set of (3.2), means that β_1 is real and has the same sign as r_1^2. One also finds that the *imaginary* part of this equation is a consequence of the other equations and should be discarded. Thus, in such a situation one actually uses (3.1) with $\gamma_1 = 0$ and β_1 real, so that

https://doi.org/10.1017/S0956792597003057 Published online by Cambridge University Press

there are $2N-2$ complex parameters β_j and γ_j for $j = 2, \ldots, N$ and one real parameter β_1. To solve for these, we have the $2N-2$ complex equations in (3.2) for $j = 2, \ldots, N$, together with the real part of the equation from the second set in (3.2) for $j = 1$. If any symmetry is present, this can be exploited in ways that should be evident.

The resultant system of equations can be solved by a path-following algorithm. With either of the schemes for producing a sequence of maps discussed above, whether one begins with too much injection at the correct points or injects the correct amount at points that are too close together, the initial image domain is nearly circular and one can easily estimate the parameter values sufficiently accurately to enable the equations to be solved numerically. As the amounts injected are reduced or the injection points pushed further apart, one uses previously computed values, or extrapolations therefrom, as starting values in an iterative routine for the numerical solution. As one would expect, accurate estimates become more important as the singular N-disk state is approached. Again, one should note the point made in the previous section: the numerical difficulties are alleviated by choosing the injection point to which the origin of the ζ-plane is to map to be near some notional centre of the array. For example, to produce Figure 2 one should choose to map $\zeta = 0$ to the centre of the central disk, though choosing to map it to the centre of any of the other disks will produce exactly the same curves in the final figure.

If we have an array that is symmetric about a point where two disks touch and wish to exploit this symmetry, it is this point to which the origin in the ζ-plane must be chosen to map, and not an injection point. A somewhat different approach is then needed with that symmetry reflected in the choice of parameters in (3.1), but the necessary modifications should be evident.

Whatever scheme of injection is used to approach a given N-disk configuration, note the close relationship between equations (2.8) and (3.2). The former were originally derived as a consequence in very special circumstances, but the Hele-Shaw procedure makes it evident that, with an appropriate interpretation, they are much more widely applicable.

One further result that is most easily visualized in the Hele-Shaw context will prove useful later. Let $z = \tilde{z}$ be the location of the centre of area of the domain occupied by fluid following injection at $z = a_j$ of areas πr_j^2 for $j = 1, 2, \ldots, N$. From equations (3.1) and (3.2), we find that

$$\tilde{z} \sum_{j=1}^{N} r_j^2 = \sum_{j=1}^{N} a_j r_j^2; \tag{3.3}$$

the coordinates of the centre of area are weighted means of the coordinates of the injection points, the weights being the areas injected.

4 Stokes flows

We use the notations and conventions of Richardson (1992), and refer the reader to that paper for the derivation of equations that we will simply state. Suppose the fluid to occupy a simply-connected domain in the plane of $z = x + iy$ whose entire boundary is a free surface at which a constant surface tension T acts. It will be convenient to denote the dimensional time variable by t^*, and μ is the fluid viscosity.

Let the region occupied by fluid at time t^* be the image of $|\zeta| < 1$ under the map $z = w(\zeta) = w(\zeta; t^*)$; the time variable will generally not be recorded explicitly in our notation.

https://doi.org/10.1017/S0956792597003057 Published online by Cambridge University Press

If we suppose that the boundary of the fluid region is an analytic curve, as it will be except in the singular initial states, then $w(\zeta)$ is analytic for $|\zeta| \leqslant 1$. The conformal nature of the map implies that $w'(\zeta) \neq 0$ for $|\zeta| < 1$; we suppose in the following that $w'(\zeta) \neq 0$ for $|\zeta| \leqslant 1$, though we know that zeros of $w'(\zeta)$ tend to points on $|\zeta| = 1$ as we approach the initial states of interest to us, and we will find that they can do so in other circumstances too.

Two functions $F_+(\zeta)$ and $F_-(\zeta)$ are defined by the decomposition

$$\frac{1}{\{w'(\zeta)\,\bar{w}'(1/\zeta)\}^{1/2}} = F_+(\zeta) - F_-(\zeta), \tag{4.1}$$

where $F_+(\zeta)$ is analytic for $|\zeta| \leqslant 1$, while $F_-(\zeta)$ is analytic for $|\zeta| \geqslant 1$ with $F_-(\zeta) \to 0$ as $\zeta \to \infty$. Here we are using the notation of the conjugate function: the analytic function $\bar{f}(\zeta)$ is defined in terms of the analytic function $f(\zeta)$ by $\bar{f}(\bar{\zeta}) = \overline{f(\zeta)}$, so that $\bar{f}(\zeta)$ and $f(\zeta)$ have regions of analyticity that are reflections of each other in the real axis. We have the representation

$$F_+(\zeta) = \frac{1}{2\pi i}\int \frac{1}{\{w'(\tau)\,\bar{w}'(1/\tau)\}^{1/2}} \frac{d\tau}{\tau - \zeta} \quad \text{for} \quad |\zeta| < 1, \tag{4.2}$$

where the integration is round the unit circle $|\tau| = 1$ traversed anticlockwise. $F_-(\zeta)$ is given by the same expression as on the right-hand side of (4.2) for $|\zeta| > 1$, and both $F_+(\zeta)$ and $F_-(\zeta)$ can be continued analytically outside the regions where these formulae can serve as definitions.

The functions $\Phi(\zeta)$ and $X(\zeta)$ that appear below are analytic for $|\zeta| \leqslant 1$, but we do not need to recall their origin here.

The two equations we require are (2.18) and (2.19) in Richardson (1992), namely

$$\Phi(\zeta) + \frac{T}{2\mu} F_+(\zeta)\,\zeta w'(\zeta) = -w(\zeta)\frac{\bar{\Phi}'(1/\zeta)}{\bar{w}'(1/\zeta)} - \bar{X}(1/\zeta) + \frac{T}{2\mu} F_-(\zeta)\,\zeta w'(\zeta) \tag{4.3}$$

and

$$\frac{\partial w}{\partial t^*}(\zeta;\, t^*) = 2\Phi(\zeta) + \frac{T}{2\mu}[2F_+(\zeta) - F_+(0)]\,\zeta w'(\zeta;\, t^*). \tag{4.4}$$

Some conditions are necessary for these equations to be correct, the most important of which is that we must have $w(0) = w(0;\, t^*) = 0$ for all t^*. This is just a mathematical condition of no physical significance, but is linked to the requirement $\Phi(0) = 0$ which is used for mathematical convenience, but singles out a particular translatory component to the entire motion in the z-plane. To obtain the form of equation (4.4) given, we must also exploit an appropriate rotation of the ζ-plane but, by accepting a particular rotational component to the entire motion in the z-plane, we may continue to impose the convenient condition $w'(0;\, t^*) > 0$ for all t^*.

The separate equations (4.3) and (4.4) are used by Richardson (1992) to justify the logic of his approach. If at some time $w(\zeta)$ is rational (or a polynomial), then so is the combination of functions on the left-hand side of (4.3) at that time. But this combination also appears on the right-hand side of (4.4), which means that $w(\zeta)$ must remain rational (or a polynomial) as the geometry changes. However, once the rationale has been established, the function $\Phi(\zeta)$ is of no concern if it is only the evolution of the geometry

https://doi.org/10.1017/S0956792597003057 Published online by Cambridge University Press

that interests us, so it is then sensible to eliminate $\Phi(\zeta)$ between equations (4.3) and (4.4), a step taken by Cummings *et al.* (1997). The result is most conveniently expressed in terms of the function

$$G_+(\zeta) = F_+(\zeta) - \tfrac{1}{2}F_+(0); \tag{4.5}$$

note that $G_+(\zeta)$ here is the function $F(\zeta, t)$ introduced by Hopper (1990) in his equation (14). A representation of $G_+(\zeta)$ that is convenient for computations is

$$G_+(\zeta) = \frac{1}{4\pi}\int_0^{2\pi} \frac{1}{|w'(\mathrm{e}^{i\theta})|}\frac{\mathrm{e}^{i\theta}+\zeta}{\mathrm{e}^{i\theta}-\zeta}\,d\theta \quad \text{for} \quad |\zeta| < 1. \tag{4.6}$$

The elimination of $\Phi(\zeta)$ between (4.3) and (4.4) yields

$$\frac{\partial}{\partial t^*}[w'(\zeta)\,\bar{w}(1/\zeta)] + 2X(\zeta)\,w'(\zeta) = \frac{T}{\mu}\frac{\partial}{\partial\zeta}[\zeta w'(\zeta)\,\bar{w}(1/\zeta)\,G_+(\zeta)], \tag{4.7}$$

which is essentially equation (21) of Hopper (1990).

If the initial states of interest are those corresponding to an array of N touching circular disks, we now know that $w(\zeta)$ must have the form given in (3.1) which we repeat here for convenience as

$$w(\zeta) = \sum_{j=1}^{N} \frac{\bar{\beta}_j\,\zeta}{1-\bar{\gamma}_j\,\zeta}, \tag{4.8}$$

where the $2N$ parameters β_j and γ_j for $j = 1, 2, \ldots, N$, with $|\gamma_j| < 1$, now depend on time; these are referred to as *partial fraction maps* by Hopper (1990). Thus, the region occupied by fluid in such a sintering problem can always be produced by injecting fluid in the Hele-Shaw analogue at N suitable points.

The only singularities of the right-hand side of (4.7) in $|\zeta| < 1$ are poles at $\zeta = \gamma_j$ and the residues there must vanish. Equating these residues to zero on the left-hand side, we obtain

$$\frac{\mathrm{d}}{\mathrm{d}t^*}[\beta_j\,w'(\gamma_j)] = 0 \quad \text{for} \quad j = 1, 2, \ldots, N. \tag{4.9}$$

Thus the combinations $\beta_j\,w'(\gamma_j)$ are invariants, and if $\zeta = 1/\bar{\gamma}_j$ is a pole that emerges from a disk of radius r_j in the initial N-disk configuration, we have

$$\beta_j\,w'(\gamma_j) = r_j^2 \quad \text{for} \quad j = 1, 2, \ldots, N. \tag{4.10}$$

In the Hele-Shaw analogue, the injection points move, but the amounts to be injected remain the same.

If we compare coefficients of $(\zeta-\gamma_j)^{-2}$ on both sides of (4.7), we obtain a result that is most neatly written in terms of the new time variable

$$t = \frac{T}{\mu}t^* \tag{4.11}$$

as

$$\frac{\mathrm{d}\gamma_j}{\mathrm{d}t} = -\gamma_j\,G_+(\gamma_j) \quad \text{for} \quad j = 1, 2, \ldots, N. \tag{4.12}$$

Equations (4.9) and (4.12) here are equivalent to equations (31) and (30) of Hopper (1990), though his formulation of (4.9) makes it less evident that these equations can be integrated. This fact has, however, been noted by Klein Obbink (1995).

https://doi.org/10.1017/S0956792597003057 Published online by Cambridge University Press

The differential equations (4.12) govern the motion of the images in the ζ-plane of the injection points in the Hele-Shaw analogue, rather than the injection points themselves; see the first set of equations in (3.2). Note that the jth equation in (4.12) is not just a simple ordinary differential equation for γ_j alone. This is an illusion created by the condensed notation; from equations (4.6) and (4.8) we see that the right-hand side of this jth equation depends on all of β_k and γ_k for $k = 1, 2, \ldots, N$.

In a general situation, the number of parameters to be determined in the map (4.8) can be reduced from $2N$ to $2N-1$ by a similar argument to that allowing such a reduction in (3.1) in the Hele-Shaw context. Noting that the integrand in (4.6) is the product of a positive quantity and a special bilinear function, it is easy to show that the functions $G_+(\gamma_j)$ in (4.12) have a positive real part. Thus, if $\gamma_j \neq 0$ then $|\gamma_j|$ decreases; the images of the injection points in the ζ-plane have a radial component of velocity *towards* the origin. We are free to choose, say, $\gamma_1 = 0$ at some initial time with the consequence that $\gamma_1 = 0$ for all time, and the first equation of the set (4.12) becomes redundant. We can also choose $\beta_1 > 0$ for all time (note that in the present situation we have $r_1^2 > 0$) and then, as for the Hele-Shaw flows, the imaginary part of the equation with $j = 1$ in (4.10) is also redundant. We thus have 1 real and $2N-2$ complex parameters in the map, to be determined from 1 real and $N-1$ complex algebraic equations, plus $N-1$ complex differential equations. Any symmetry that is present can be exploited to reduce the number of variables and equations, or to justify assuming them to be real, or to introduce a combination of these simplifications, as appropriate.

When the problem is symmetric about a point where two disks touch, the choice $\gamma_1 = 0$ is still possible but fails to take advantage of this symmetry. A different choice with the symmetry reflected in the parameters in (4.8) is then more prudent.

If we wish to consider an initial state with some given N-disk configuration, we need to begin the integrations required in (4.12) with appropriate values of the β_j and γ_j that correspond to a geometry sufficiently close to this singular beginning. A natural approach is to exploit the results of an asymptotic analysis, but the developments in §2 indicate that, for all but the simplest of scenarios, this will be a daunting task. Moreover, such results as have been obtained thus far are disappointing. For example, both Hopper (1992) and van de Vorst (1994) obtain the first few terms of pertinent expansions for the simplest case of the coalescence of two equal circular cylinders, but these expansions entail either powers of logarithms or logarithmic integrals, and their accuracy leaves much to be desired. It is here that the Hele-Shaw analogue proves invaluable as a practical aid. To obtain the starting values for the sintering problem, we operate as indicated in §3, injecting the correct amounts at N points near to each other to begin with, and approach the N-disk configuration as closely as desired by pushing the injection points apart, keeping the amounts injected fixed, a constraint that we now know to be *precisely* that relevant for the motion induced by sintering.

A further point should be made concerning the initial-value problem posed by the N-disk configuration: from both a mathematical and a physical standpoint, it is ill-posed. If we choose the scheme with $\gamma_1 = 0$, then $\mathrm{Re}\{G_+(\gamma_j)\} \to 0$ for $j \neq 1$ as the N-disk configuration is approached, and we have the classic non-uniqueness problem encountered in the theory of differential equations: see Example 3 in §2.3 of Hille (1969), for instance. One solution has the γ_j remaining at their initial values for ever; others have each $|\gamma_j|$ for $j \neq 1$ remaining

https://doi.org/10.1017/S0956792597003057 Published online by Cambridge University Press

at the value 1 for some interval of time before beginning to decrease. This merely reflects some experimental difficulties: even with just two disks, it would seem to be impossible to locate the instant when coalescence commences precisely. With more than two disks, how can we ensure that coalescence between all pairs of touching disks commences at the same instant?

In the examples of the next section, we have adopted a uniform strategy. All the starting configurations were obtained via the Hele-Shaw analogy with the injection points forming touching disks a distance apart precisely 10^{-4} less than the distance between their centres. The neck between two such disks then has a width of order 10^{-2}, while the curvatures there are order 10^{6}. The angular relationship between the injection points was, of course, the same as that between the centres. This initial state corresponds to our time origin $t = 0$, a point to be borne in mind when values of t are quoted later.

For examples that approach a single circular disk as $t \to \infty$, an attempt has been made to introduce some order into the choice of values of t for which the outlines are plotted to give some indication of the rates of change at different times and positions. The fact that the geometry evolves relatively slowly when t is large is compensated for by using a scaling involving the tangent function, but other influences intrude too. One of these is that, convenient though it may be, the time variable t defined in (4.11) actually has the dimensions of a length! Also, the relevant length scale is different in different phases of any given motion. As a compromise, sketches are drawn by setting $t = A \tan v$, taking seven equal increments in v from 0 to $\pi/2$, and choosing the number A for each figure to give an acceptable spacing of the curves drawn.

As already noted, the convenient choice $w(0) = 0$ for the theory generally imposes a translation on the motion in the z-plane that is outside our control. An instructive example of this arises if we take $N = 1$ in (4.8) with $\gamma_1 \neq 0$; this is then a bilinear map yielding a circular disk in the z-plane whose centre is not at the origin. The mathematical solution has γ_1 approaching the origin in the ζ-plane as $t \to \infty$, and the circular disk in the z-plane translates with its centre approaching the origin there while its radius remains fixed – a motion of no physical significance. Where appropriate in the figures, such an irrelevant translation has been removed by shifting all the centres of area to a common point before plotting, a step that is easily accomplished with the aid of equation (3.3).

The condition $w'(0) > 0$ we use also fixes a rotational component of the motion in the z-plane, and different choices of origin can affect this component. Bearing in mind the advice in §2 that the origin should be chosen to minimize the numerical difficulties caused by the singularities while taking advantage of any symmetry, there is generally just one sensible choice of origin. Only when there may be some doubt and a different apparently sensible choice would produce a slightly different picture do we state the origin used for the calculations.

5 Examples

Figure 3 shows the coalescence of two unequal circular disks, the radii being $r_1 = 2$ and $r_2 = 1$. The outlines are those from the Hele-Shaw analogue with injection of area 4π and π at injection points whose distance apart decreases from 3 to 0, with the centre of area kept fixed. In fact, the calculation need not refer to this analogue except, recall, that we have chosen to take $t = 0$ when these injection points are a distance 2.9999 apart. We have

https://doi.org/10.1017/S0956792597003057 Published online by Cambridge University Press

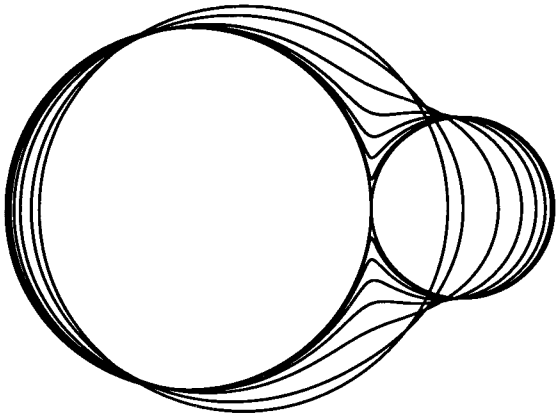


FIGURE 3. The coalescence of two circular disks of radii 2 and 1 to form a single circular disk of radius $\sqrt{5}$. With $t = \tan v$, the outlines are drawn for seven equal increments in v from 0 to $\pi/2$.

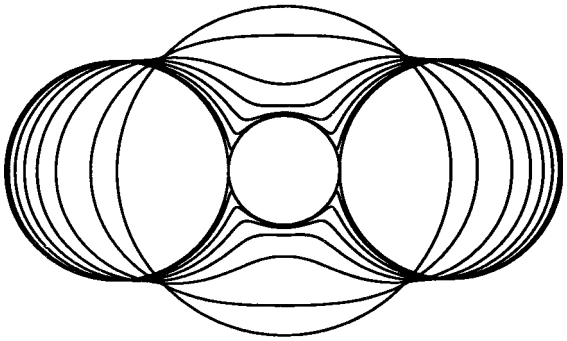


FIGURE 4. The coalescence of three circular disks, one of radius 1 and two of radius 2, to form a single circular disk of radius 3; the centres of the disks are collinear. With $t = 1.3 \tan v$, the outlines are drawn for seven equal increments in v from 0 to $\pi/2$.

$N = 2$ and $\gamma_1 = 0$ in (4.8), while γ_2, β_1 and β_2 are all real and positive with the usual conventions. As γ_2 decreases from 1 to 0, we solve the two real equations in (4.10) for β_1 and β_2 to determine the outlines – or, rather, we initially perform the calculations as γ_2 *increases* from 0 to 1 so that we can begin the path-following routine from a situation where β_1 and β_2 are easy to estimate. The numerical integration of the single differential equation from (4.12) with $j = 2$ then links a particular t to a particular outline.

In this simple case one can actually solve the two equations in (4.10) explicitly for β_1 and β_2 as functions of γ_2, and similar variations on the procedure are possible in some of our other examples. In this 2-disk situation, it is also true that the function $G_+(\gamma_2)$ can be expressed in terms of elliptic integrals (as can the corresponding integrals in the more complicated formulae of Richardson, 1992), but the modulus involved does not appear to be simply related to the parameters in the map unless the disks are of the same radius, and the determination of $G_+(\gamma_2)$ by numerical means using equation (4.6) seems preferable. The present results can, of course, be shown to agree with those of Richardson (1992).

Adding a further circular disk of radius 2 on the right to the initial 2-disk configuration in Figure 3, we obtain the motion in Figure 4. One expects the initial behaviour near where

https://doi.org/10.1017/S0956792597003057 Published online by Cambridge University Press

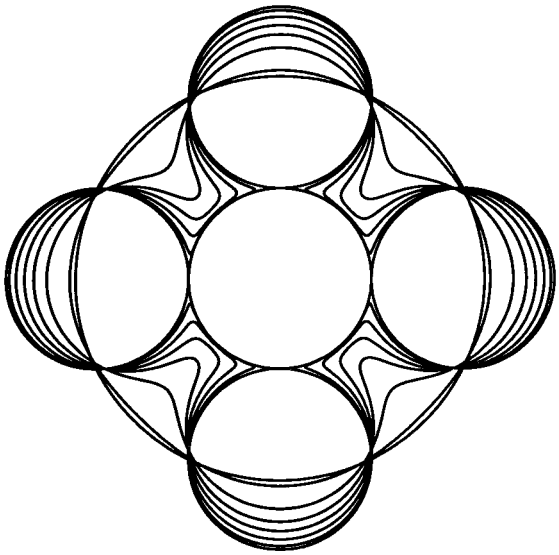


FIGURE 5. The coalescence of five circular disks all of radius 1, four of them being symmetrically placed round a central one. With $t = 0.9 \tan v$, the outlines are drawn for seven equal increments in v from 0 to $\pi/2$.

two disks touch to be essentially the same in both cases, and one should note that the global constraint applied to keep the centres of area fixed affects the appearance of the sketches in this region. Again, because of the symmetry, the Hele-Shaw analogue shows that the curves here are obtained simply by solving algebraic equations, with the numerical integration needed only to determine the time variation; we have injection of areas 4π at each of two points moving symmetrically towards a third point at which an area π is injected.

In Figure 5, the initial configuration has five circular disks all of radius 1, with four of the disks evenly spaced round a central one. Again, because of the symmetry, the evolution of the geometry is determined by purely algebraic equations.

Figure 5 provokes some thoughts. If we keep the radius of the central disk as 1 but increase the radius of all four outer ones together, these actually touch in the initial state when their radius has reached the value $1 + \sqrt{2} = 2.414$. One might expect that the evolution itself would eventually produce a similar touching state if we begin with outer disks of radius a little less than this value, and this is indeed the case. Figure 6 shows the situation when the outer disks are of radius 2; only one quarter of the entire fluid region is shown so that a portion of particular interest can be drawn larger. To follow the motion beyond the instant when the boundary touches itself requires a different solution procedure from the one developed in this paper, for the region occupied by the fluid is then no longer simply-connected.

But what happens on the borderline between the two types of behaviour illustrated in Figures 5 and 6? The reasoning is precisely that used by Richardson (1996b, 1997b) to produce examples of Hele-Shaw flows with *zero* surface tension that have the free boundary passing through a cusped state, and the conclusion here is the same; we now have a Stokes flow with *non-zero* surface tension for which the free boundary passes through a cusped

https://doi.org/10.1017/S0956792597003057 Published online by Cambridge University Press

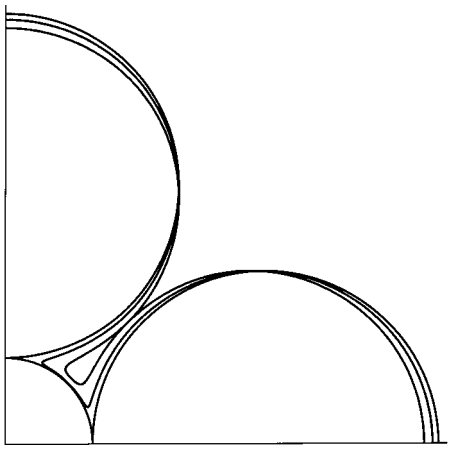


FIGURE 6. Five disks as in Figure 5, but the outer ones are of radius 2 while the central one is still of radius 1. With an origin in the middle of the array and all the centres of the disks on the axes of a Cartesian coordinate system, only the picture in the first quadrant is shown. The free boundary touches itself when $t = t_1 = 0.674$ at the point (1.408, 1.408). The boundary is drawn for $t = \frac{1}{2}t_1$ and $t = t_1$.

state. In fact, the symmetry present in the current context allows the conditions necessary for this to occur to be determined analytically.

We now have, as for Figures 5 and 6, five disks and $N = 5$ in (4.8), with $\gamma_1 = 0$. Placing the centres of the disks along the axes in the z-plane, we have $\beta_1 > 0$ while the β_j for $j = 2, 3, 4, 5$ are all equal to some $\beta > 0$. The four γ_j for $j = 2, 3, 4, 5$ are equal to $\pm\gamma$, $\pm i\gamma$ for some $\gamma > 0$, so that the map (4.8) contains only three parameters to be determined. Correspondingly, equations (4.10) provide just two real equations.

In the cusped state we seek to determine, the cusps correspond to $\zeta = e^{i\pi/4}$, plus three symmetrically disposed points. The conditions to be imposed follow as in Richardson (1996 b) and are

$$w'(\zeta) = 0 \quad \text{and} \quad \mathrm{Re}\left\{\zeta\frac{w'''(\zeta)}{w''(\zeta)}\right\} = -3 \quad \text{for} \quad \zeta = e^{i\pi/4}. \tag{5.1}$$

With the central disk of radius $r_1 = 1$, equations (5.1) and the two equations from (4.10) can be solved to show that the borderline state with the cusp that lies between Figures 5 and 6 occurs when the outer disks are of radius $r_2 = \sqrt{(13+5\sqrt{5})/8} = 1.739$. At the instant when the cusps are present, we find that $\beta_1 = \beta = 1/\sqrt{5} = 0.447$ and $\gamma = (5-2\sqrt{5})^{1/4} = 0.852$, and the numerical integration of the single equation that emerges from (4.12) indicates that this occurs when $t = t_2 = 1.22$; recall our convention concerning the origin of time which here means that $t = 0$ corresponds to the state produced by injection in the Hele-Shaw analogue of an area $\pi r_1^2 = \pi$ at the origin and an area πr_2^2 at four points a distance $r_1 + r_2 - 10^{-4}$ away from the origin along the axes. The motion of the free boundary in this critical situation is sketched in Figure 7. As a curiosity, I record that the distance of the cusps from the centre of the array when they form is $(1+\sqrt{5})/2 = 1.618$ which is, of course, the golden ratio.

https://doi.org/10.1017/S0956792597003057 Published online by Cambridge University Press

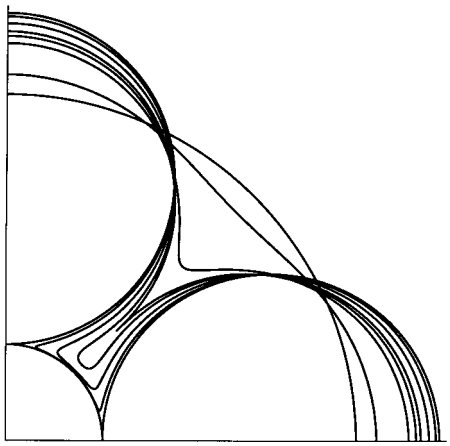


FIGURE 7. Five disks as in Figures 5 and 6, but the outer ones are of radius $\sqrt{(13+5\sqrt{5})/8} = 1.739$ while the central one is still of radius 1; as in Figure 6, only the first quadrant is shown. The free boundary passes through a cusped configuration when $t = t_2 = 1.22$. With $t = A\tan v$, the outlines are drawn for seven equal increments in v from 0 to $\pi/2$, and A is chosen so that the fourth increment yields $t = t_2$.

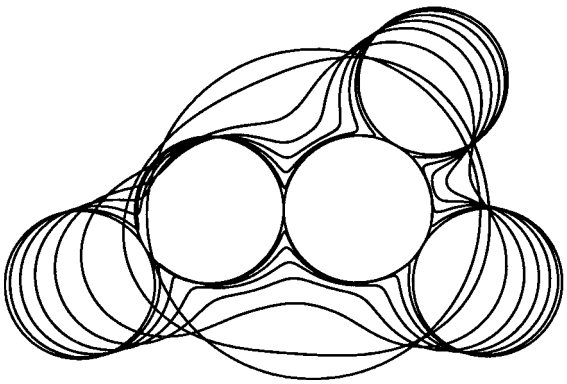


FIGURE 8. The coalescence of five circular disks, all of radius 1. Their centres are at $z = 0$, $2\,e^{i\pi/3}$, -2, $-2-2\,e^{i\pi/6}$ and $2\,e^{-i\pi/6}$. With $t = \tan v$, the outlines are drawn for seven equal increments in v from 0 to $\pi/2$.

The present example should be compared with those of Howison & Richardson (1995) and Tanveer & Vasconcelos (1994, 1995), where the inclusion of a non-zero surface tension in some Stokes flow problems is shown to prevent the formation of cusps that *do* appear when the surface tension is taken to be zero. In particular, the nature of the cusps here is quite different. To use the customary descriptions, it seems that, while surface tension may keep at bay the 3/2-power cusps, it does not prevent the appearance of 5/2-power cusps. Note, too, that the near-cusps occurring in the earlier works arise as a consequence of an imposed suction mechanism, while the genuine cusps here evolve in a motion driven solely by surface tension. While the near-cusps persist once formed (but disappear if the suction is removed), the free boundary here passes *through* the cusped state.

Figure 8 shows an example involving five initial disks, all of radius 1, that possesses no symmetry. Following the advice in §2, the origin during the calculations has been chosen

https://doi.org/10.1017/S0956792597003057 Published online by Cambridge University Press

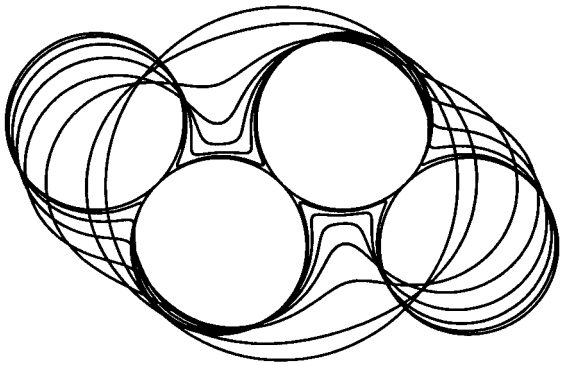


FIGURE 9. The coalescence of four circular disks, all of radius 1. Their centres are at $z = \pm e^{i\pi/4}$ and $\pm(e^{i\pi/4} + 2\,e^{-i\pi/4})$. With $t = \tan v$, the outlines are drawn for seven equal increments in v from 0 to $\pi/2$.

at the centre of the disk that is third from the left, so that the initial state is treated as this disk with two separate disks and a 2-disk array grafted on to it.

Figure 9 shows an example involving four initial disks, all of radius 1, that is symmetric about a point where two disks touch, so it is sensible to use this point as the origin during the calculations. A similar choice is also prudent when the symmetry is about a line that passes through such a point, as is the case, for example, when we have four touching disks of radius 1 with their centres on a circle of some radius greater than $\sqrt{2}$.

6 Concluding remarks

All the numerical work required for this paper was performed using *Mathematica*, and its graphics facilities were employed for the production of the figures. The principal difficulties arise from the calculation of the functions $G_+(\gamma_j)$ appearing in equations (4.12) when near the initial state; these are particularly severe in the example of Figure 9 where the initial motions of the γ_j associated with the two outer disks have a substantial tangential component, but a comparatively minute inward radial component, so these γ_j at first move round only just inside the unit circle. Further difficulties arise in the example shown in Figure 7, for the cusp in this figure is produced by a zero of $w'(\zeta)$ that first approaches the unit circle $|\zeta| = 1$ and then recedes from it, so that $G_+(\gamma)$ passes through a singular state. *Mathematica* successfully negotiated such difficulties with the aid of appropriate options but, without knowing exactly what the routines invoked are doing, it is not possible to estimate the likely errors. In particular, though the values quoted for t_1 and t_2 in Figures 6 and 7 are believed to be correct to the number of digits given, this brief relies heavily on the author's faith in the abilities of *Mathematica*.

We have emphasized initial states that consist of touching circular disks because these appear to be of most interest, but it should be clear that the same procedure is applicable in other circumstances. In particular, we may consider bundles of fibres whose section is other than circular. To analyse the problem exactly, the initial section must be producible by injection and suction in the Hele-Shaw analogue, but arbitrarily close approximations to any section that is likely to arise in practice can be produced by exploiting the physical insight imparted by the analogy. Initial states relevant for the coalescence of fibres with

https://doi.org/10.1017/S0956792597003057 Published online by Cambridge University Press

circular and cardioid-like sections with cusps were effectively manufactured in Richardson (1997a), but this gives only an inkling of the range of possible variations.

It is evident that the idea exploited in Figure 7 can be used to produce many more examples of cusp formation in Stokes flow with non-zero surface tension. It also seems reasonable to suppose that the same principle would succeed when considering Hele-Shaw flows with non-zero surface tension, so that cusps may develop in these circumstances too.

References

Cummings, L. J., Howison, S. D. & King, J. R. (1997) Conserved quantities in Stokes flow with free surfaces. *Phys. Fluids* **9**, 477–480.

Hille, E. (1969) *Lectures on Ordinary Differential Equations*. Addison-Wesley.

Hopper, R. W. (1984) Coalescence of two equal cylinders: Exact results for creeping viscous plane flow driven by capillarity. *J. Am. Ceram. Soc.* (*Comm.*) **67**, C262–264.

Hopper, R. W. (1990) Plane Stokes flow driven by capillarity on a free surface. *J. Fluid Mech.* **213**, 349–375.

Hopper, R. W. (1991) Plane Stokes flow driven by capillarity on a free surface. Part 2. Further developments. *J. Fluid Mech.* **230**, 355–364.

Hopper, R. W. (1992) Stokes flow of a cylinder and half-space driven by capillarity. *J. Fluid Mech.* **243**, 171–181.

Hopper, R. W. (1993) Capillarity-driven plane Stokes flow exterior to a parabola. *Quart. J. Mech. Appl. Math.* **46**, 193–210.

Howison, S. D. & Richardson, S. (1995) Cusp development in free boundaries, and two-dimensional slow viscous flows. *Euro. J. Appl. Math.* **6**, 441–454.

Klein Obbink, B. (1995) Moving boundary problems in relation with equations of Löwner–Kufareev type. *PhD thesis*, Eindhoven University of Technology.

Richardson, S. (1968) Two-dimensional bubbles in slow viscous flows. *J. Fluid Mech.* **33**, 475–493.

Richardson, S. (1973) Two-dimensional bubbles in slow viscous flows. Part 2. *J. Fluid Mech.* **58**, 115–127.

Richardson, S. (1992) Two-dimensional slow viscous flows with time-dependent free boundaries driven by surface tension. *Euro. J. Appl. Math.* **3**, 193–207.

Richardson, S. (1996a) Hele-Shaw flows with free boundaries driven along infinite strips by a pressure difference. *Euro. J. Appl. Math.* **7**, 345–366.

Richardson, S. (1996b) Hele-Shaw flows with time-dependent free boundaries involving a concentric annulus. *Phil. Trans. R. Soc. Lond.* A **354**, 2513–2553.

Richardson, S. (1997a) On the classification of solutions to the zero-surface-tension model for Hele-Shaw free boundary flows. *Quart. Appl. Math.* **55**, 313–319.

Richardson, S. (1997b) Hele-Shaw flows with time-dependent free boundaries involving an infinite strip of fluid. *Quart. Appl. Math.* (to appear).

Tanveer, S. & Vasconcelos, G. L. (1994) Bubble breakup in two-dimensional Stokes flow. *Phys. Rev. Lett.* **73**, 2845–2848.

Tanveer, S. & Vasconcelos, G. L. (1995) Time-evolving bubbles in two-dimensional Stokes flow. *J. Fluid Mech.* **301**, 325–344.

Vorst, G. A. L. van de (1994) Modelling and numerical simulation of viscous sintering. *PhD thesis*, Eindhoven University of Technology.

https://doi.org/10.1017/S0956792597003057 Published online by Cambridge University Press